available at www.sciencedirect.com

ScienceDirect

journal homepage: www.elsevier.com/locate/chnjc

Article (Dedicated to Professor Yi Chen on the occasion of his 80th birthday)

Synthesis and catalytic activity of M@SiO_2 (M = Ag, Au, and Pt) nanostructures via "core to shell" and "shell then core" approaches

Shengchao He, Zhaoyang Fei, Lei Li, Bo Sun, Xinzhen Feng, Weijie Ji *

Laboratory of Mesoscopic Chemistry of MOE, School of Chemistry and Chemical Engineering, Nanjing University, Nanjing 210093, Jiangsu, China

ARTICLE INFO

Article history:
Received 30 August 2013
Accepted 22 September 2013
Published 20 November 2013

Keywords:
Core-shell structure
Silver
Gold
Platinum
Nanoparticle
Silica
CO oxidation
4-Nitrophenol reduction

ABSTRACT

M@SiO_2 (M = Ag, Au, and Pt) core-shell nanostructures were prepared by the "core to shell" and "shell then core" approaches. In the former, the metal core size could be controlled in the 6–9 nm range with a narrow size distribution, and the shell porosity was tunable. The preparation was straightforward and efficient, without requiring specialized high-speed centrifugation. Au@SiO_2 containing mesoporous SiO_2 shells (Au@meso-SiO_2) exhibited good thermal stability and high CO oxidation activity (T_{100} = 235 °C) even after being subjected to calcination in air at 550 °C. In the latter approach, the core size could be controlled at < 10 nm with a narrow size distribution, and the shell porosity was tunable to a fine degree. 4-Nitrophenol was readily reduced at room temperature in the presence of Au@meso-SiO_2 obtained through the "shell then core" approach. The SiO_2 shell mesoporosity minimized the diffusion limitation of 4-nitrophenol. The core-shell structures from both approaches were uniformly dispersed. Employing Si sources with differing functionality allowed the SiO_2 shell and metal core properties to be modified in these approaches, which is beneficial for application.

1. Introduction

The surface area of nanoparticles (NPs) increases rapidly with decreasing particle size. However, NPs often aggregate because of their high surface energy, especially at elevated temperatures, thus losing their inherent high surface area. Many applications require nanomaterials with multiple functionality, which in turn requires the development of hierarchical nanostructures. The synthesis of core-shell nanostructures has received much recent attention. Core-shell structured materials can be carefully designed and prepared in regards to both structure and composition. This gives them attractive properties with potential in semiconductor [1], bio-technology [2,3], and drug delivery [4,5] applications. Various core-shell nanomaterials including metal@metal [6,7], metal@oxide [8,9], metal@carbon [10,11], metal@polymer [12,13], and metal@zeolite [14–16] structures have been developed and used in catalysis [17].

SiO_2 is widely available and frequently used as a coating material. SiO_2 is highly stable and can protect metal core particles from aggregation, while the SiO_2 shell porosity can be systematically modified. Functional groups such as $-NH_2$, –OH, and –COOH are easily attached to the SiO_2 shell surface, which facilitates their potential in biological applications. The SiO_2 shell is well suited for tuning the surface properties of metal core particles. SiO_2 encapsulated metal NPs are extensively applied in colloid and materials science [18–20]. Core-shell structures of different shapes and core sizes have been synthesized via the

* Corresponding author. Tel: +86-25-83686270; Fax: +86-25-83317761; E-mail: jiwj@nju.edu.cn
This work was supported by the National Natural Science Foundation of China (21173118), the Natural Science Foundation of Jiangsu Province (BK2011439), the Specialized Reaearch Fund for the Doctoral Program of High Education (20110091110023), and the National High Technology Research and Development Program of China (863 Program, 2013AA031703).
DOI: 10.1016/S1872-2067(12)60716-5 | http://www.sciencedirect.com/science/journal/18722067 | Chin. J. Catal., Vol. 34, No. 11, November 2013

sol-gel approach [18,21,22]. Fe_2O_3 [23], ZrO_2, and TiO_2 [24] NPs obtained by liquid phase synthesis contain significant surface –OH groups, and SiO_2 shells are readily deposited on these oxide NPs via the hydrolysis-condensation route. The SiO_2 shell encapsulation of the metal core NPs is only satisfactory after the core hydrophilicity is enhanced by specific protective and/or modifying agents and Si-coupling agents. Thus, the synthetic process is often complicated and difficult to apply to the fabrication of other NPs. Graf et al. [25] prepared core-shell metal NPs using polyvinylpyrrolidone (PVP) as a decorating agent. This methodology is also suitable for preparing Au, Ag@SiO_2, and Al_2O_3@SiO_2 core-shell structures. It is difficult to form core-shell structures from metal NPs with diameters of < 8 nm. Gorelikov et al. [26] synthesized aqueous metal@SiO_2 materials using cetyltrimethylammonium bromide (CTAB) as a stabilizing and structure-directing agent. The resulting materials were easily dispersed, and their mesoporous SiO_2 shells were well suited to fast mass transport. However, this synthetic method is time-consuming and requires specialized high-speed centrifugation. Well-dispersed core-shell metal NPs were recently prepared via anti-phase microemulsion [27]. The SiO_2 shell thickness was controllable; however, the method required excess organic solvent and surfactant, resulting in high production costs and tedious post treatment.

Huang et al. [21] prepared 6.3 nm diameter Au NPs in the organic phase using mercaptoundecyl as a stabilizing agent. By further employing 11-mercaptoundecanoic acid (MUA) as a surface decorating agent to enhance the Au NP hydrophilicity, they produced core-shell Au@SiO_2 via a modified Stöber method. One strategy of the current study is to use MUA as both a stabilizing and decorating agent (free of mercaptoundecyl) to prepare Au NPs in ethanol. We aim to directly encapsulate Au NPs with SiO_2 in water/ethanol through a supersonic-assisted Stöber process.

Core-shell structures are generally synthesized following the above-mentioned "core to shell" approach. The small particle sizes and high surface energies mean that the colloidal metal sol concentration is usually low, and thus productivity is inefficient. A new "shell then core" route has recently been reported, in which the SiO_2 shell is prepared, and the metal core subsequently introduced. Hah et al. [28,29] employed phenyl trimethyl silane as a Si source and carefully adjusted the pH to form hollow SiO_2 spheres. The hollow SiO_2 spheres were then filled with $Cu(NO_3)_2$ solution by supersonic-assisted impregnation. Cu^{2+} inside the spheres was reduced to Cu^0 using hydrazine. Repeating these impregnation-reduction steps allowed the gradual growth of Cu^0 core particles. $Cu(NO_3)_2$ also existed inside and outside the hollow SiO_2 spheres and was also reduced by hydrazine. This caused an uneven distribution of Cu^0 particles inside and outside the shells. Chen et al. [30] and Tan et al. [31] recently modified the "shell then core" approach. They employed *N*-(3-(trimethoxysilyl)propyl)ethylenediamine (TSD) and tetraethylorthosilane (TEOS) Si sources to prepare core-shell SiO_2@TSD and SiO_2@SiO_2. The medium layer was then etched by HF to produce yolk-shell SiO_2@SiO_2, which was further subjected to HF etching to generate hollow SiO_2 spheres. In this route, there were significant ethylenediamine groups on the inner surface of SiO_2 shells, with which the $HAuCl_4$ precursor could be in-situ reduced to Au NPs. The Au NP size could be changed by varying the $HAuCl_4$ concentration. This procedure required multiple Si sources and the use of HF, which brings about technical complications and safety issues. The second strategy of the current study is to directly prepare hollow SiO_2 spheres by avoiding HF and to introduce Ag and Au cores by in-situ reduction.

The current study aims to prepare monodisperse Pt, Au, and Ag@SiO_2 core-shell nanostructures through simple and efficient "core to shell" and "shell then core" approaches. These methods are low cost and versatile for preparing metal@SiO_2 structures. M@SiO_2 (M = Ag, Au, and Pt) were obtained through the two approaches, and the catalytic properties of Au@SiO_2 were investigated. For Au@SiO_2 containing mesoporous SiO_2 shells (Au@meso-SiO_2) prepared through the "core to shell" route, a gas-solid heterogeneous CO oxidation was used as the model reaction to understand the stability of Au@SiO_2. For Au@meso-SiO_2 prepared through the "shell then core" approach, a liquid-solid heterogeneous 4-nitrophenol (4-NP) reduction was used to investigate the diffusion limitation of reactant through the mesoporous SiO_2 shell.

We have previously prepared Fe_2O_3, NiO, Co_3O_4, and RuO_2 NPs as core precursors for encapsulation by SiO_2, Al_2O_3, and MgO. M@SiO_2, Al_2O_3, and MgO (M = Fe, Ni, Co, Ru) core-shell nanostructures were obtained by in-situ hydrogen reduction and applied in ammonia decomposition and methane oxygen reforming for CO_x free H_2 and syngas production [32–36]. The current study involves the direct encapsulation of metal core NPs in contrast to our previous studies.

2. Experimental

2.1. "Core to shell" strategy

Metal NPs were first prepared through liquid phase reduction in the presence of protective and surface decorating agents. SiO_2 encapsulation was then achieved following a modified Stöber process. MUA was used as a protective/surface decorating agent to stabilize the dispersed Au, Ag, and Pt NPs in the ethanol/water. MUA also induced the deposition of SiO_2 shells on the metal NP surface. Octadecyltrimethoxysilane (C_{18}TMS) was used to modify the SiO_2 shell texture and consequently to modify the shell diffusion properties.

2.1.1. Ag@SiO_2 preparation

$AgNO_3$ (4 mg) and MUA (1 mg) in ethanol (30 ml) were stirred at room temperature (RT) for 10 min. Freshly prepared $NaBH_4$ solution (5 ml, 8.0×10^{-2} mol/L) was added under rigorous stirring. The color quickly changed to reddish orange, indicating the formation of Ag NPs. $NH_3\cdot H_2O$ (2 ml) and H_2O (10 ml) were added under stirring until the mixture was clean. A solution containing TEOS (0.5 ml) in ethanol (10 ml) was then slowly added, and the mixture was stirred for 6 h. The resulting colloidal sol was dried at 80 °C for 3 h.

2.1.2. Pt@SiO_2 preparation

$H_2PtCl_6 \cdot 6H_2O$ solution (1 ml, 1.93×10^{-2} mol/L) and MUA (0.5 mg) in ethanol (30 ml) were stirred at RT for 10 min. Freshly prepared $NaBH_4$ solution (4.5 ml, 8.0×10^{-2} mol/L) was added under rigorous stirring. The color changed to deep brown, indicating the formation of Pt NPs. NaOH (2 ml, 0.625 mol/L) was added, and the solution was stirred for 10 min, during which time a precipitate formed. Upon centrifugation (4000 r/min, 5 min) or resting (30 min), the precipitate was isolated and was mixed with $NH_3 \cdot H_2O$ (2 ml), H_2O (10 ml), and ethanol (30 ml). The resulting mixture was stirred for 30 min. A solution containing TEOS (0.5 ml) in ethanol (10 ml) was slowly added, and the mixture was stirred for 6 h. The resulting colloidal sol was dried at 80 °C for 3 h.

2.1.3. Au@SiO_2 preparation

$HAuCl_4 \cdot 4H_2O$ solution (2 ml, 9.7×10^{-3} mol/L) and MUA (2.0 mg) in ethanol (30 ml) were stirred at RT for 10 min. Freshly prepared $NaBH_4$ solution (5 ml, 8.0×10^{-2} mol/L) was added under rigorous stirring. The color changed to claret, indicating the formation of Au NPs. NaOH solution (2 ml, 0.625 mol/L) was added, and the solution was stirred for 10 min, during which time a precipitate formed. Upon centrifugation (4000 r/min, 5 min) or resting (30 min) the precipitate was isolated and was mixed with $NH_3 \cdot H_2O$ (2 ml), H_2O (10 ml), and ethanol (30 ml). The resulting mixture was stirred for 30 min. A solution containing TEOS (0.5 ml) in ethanol (10 ml) was slowly added, and the mixture was stirred for 6 h. The resulting colloidal sol was dried at 80 °C for 3 h.

2.1.4. SiO_2 shell modification

The same steps were adopted for preparing Au@micro-SiO_2 and Pt@micro-SiO_2 except for the last step, in which a certain amount of octadecyltrimethoxysilane (C_{18}TMS) was added with TEOS to modify the SiO_2 shell porosity.

2.2. "Shell then core" strategy

SiO_2 hollow nano-spheres were prepared by microemulsion. Upon decoration with another Si source, mesoporous SiO_2 hollow spheres with reductive functional groups were obtained. Au and Ag core NPs were finally introduced through in-situ reduction.

2.2.1. Preparation of hollow SiO_2 spheres

Hollow SiO_2 spheres were prepared in the aqueous phase as previously reported [37]. In brief, CTAB (0.2 g), C_{12}-SH (40 μl), and NaOH solution (0.7 ml, 2 mol/L) in H_2O (100 ml) was heated to 80 °C and stirred for 30 min. A solution containing TEOS (2 ml) and TSD (0.1 ml) in ethanol (5 ml) was added slowly, and a white colloidal sol formed. After stirring for 3 h, the solids were isolated, dried at 100 °C, and stored for later use.

2.2.2. Au@SiO_2 preparation

$HAuCl_4$ solution (4 ml, 9.71×10^{-3} mol/L) was added to hollow SiO_2 spheres (0.2 g) dispersed in H_2O (50 ml). The mixture was subjected to supersonic treatment of 1 h and then rested at 80 °C for 3 h. The color changed to purplish red. The solids were isolated by centrifugation (4000 r/min, 5 min) and dried at 100 °C.

2.2.3. Ag@SiO_2 preparation

Hollow SiO_2 spheres (0.2 g) were dispersed in a mixture of H_2O (50 ml) and ethanol (5 ml), and $AgNO_3$ (0.1 g) was added. The mixture was subjected to supersonic treatment and then rested at 80 °C for 12 h. The color changed to deep yellow. The solids were isolated by centrifugation (4000 r/min, 30 min) and dried at 100 °C.

2.3. Characterization

Brunauer-Emmett-Teller (BET) measurements were performed on a NOVA-1200 apparatus at −196 °C. Prior to N_2 sorption measurements, samples were degassed at 300 °C for 3 h. X-ray diffraction (XRD) patterns were collected on a Philips X'Pert MPD Pro X-ray diffractometer with Cu K_α radiation (λ = 0.1541 nm) operated at 40 kV and 40 mA. The scanning speed was 0.02° and the 2θ range was 10°–80°. Transmission electron microscopy (TEM) images were recorded on a JEM-1010 microscope operated at 80 kV.

2.4. Catalytic activity

Catalyst (50 mg, 20–40 mesh) was used for CO oxidation experiments. The feed gas was 1.4% CO in air (v/v) with a flow rate of 25 ml/min and gas hourly space velocity (GHSV) of 30000 $cm^3\ h^{-1}\ g_{cat}^{-1}$. Prior to reaction, samples were calcined in air at 550 °C for 2.5 h. The off-gas was analyzed by an on-line gas chromatograph (GC, GC122) with a packed Poropak Q column and a thermo-conductive detector.

For 4-NP reduction, Au@SiO_2 (10 mg) was dispersed in H_2O (5 ml) at RT, and $NaBH_4$ solution (1 ml, 0.3 mol/L) was added to the suspension under stirring (10 min). A 4-NP solution (0.2 ml, 7.62×10^{-2} mol/L) was added under rigorous stirring. Aliquots (0.1 ml) were removed at 3-min intervals and diluted to 4 ml with H_2O. Samples were measured on a UV-Vis spectrometer, and catalytic activity was calculated in terms of the relative absorbance at 401 nm. A blank test was performed similarly without using Au@SiO_2.

3. Results and discussion

3.1. M@SiO_2 (M = Ag, Au, and Pt) obtained through the "core to shell" approach

The surfaces of colloidal metal NPs contain few hydrophilic groups. To encapsulate them with SiO_2 shells, it is necessary to first modify them with surfactants or silicon hydride coupling agents. We adopted MUA as both a stabilizing and structure-directing agent for the colloidal metal NPs to enhance their surface hydrophilicity. This in turn facilitated the coating of SiO_2 shells on the metal core surfaces. To the best of our knowledge, this is the first report of metal NPs smaller than 10 nm prepared in ethanol directly from MUA. Figure 1 shows a

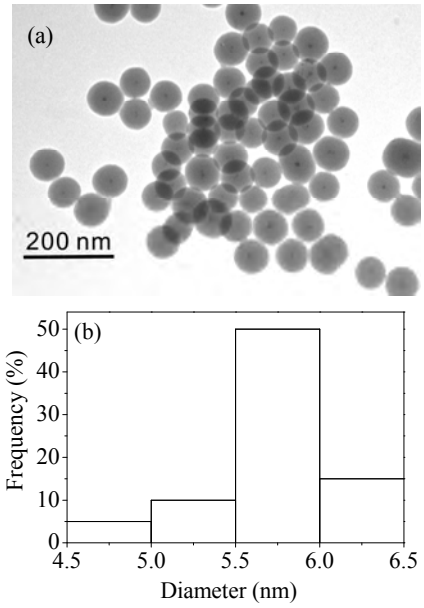

Fig. 1. TEM image of Ag@SiO_2 obtained via the "core to shell" approach (a) and the particle size distribution of Ag cores (b).

TEM image of Ag@SiO_2 particles and the corresponding Ag core size distribution. The average core size was 5.7 ± 0.5 nm, and the SiO_2 shell thickness was approximately 40–50 nm. Particles were essentially monodisperse.

To verify that the methodology was suitable for preparing other metal@SiO_2 structures, Au@SiO_2 core-shell structures were similarly fabricated. TEM images of the resulting samples with different porosity SiO_2 shells and the Au core size distribution are shown in Fig. 2. The average Au core size was 7.3 ± 1.0 nm. Multi-core encapsulation was observed in some Au@SiO_2 core-shell particles. Specifically, two to three Au NPs were encapsulated in a single SiO_2 shell in some particles, though cores remained separated by SiO_2 and did not aggregate into one large domain. Employing the C_{18}TMS agent ([C_{18}TMS]:[TEOS] = 1:8) caused the SiO_2 shell texture to become more mesoporous (apparent as loose SiO_2 shells in Fig. 2b).

N_2 adsorption-desorption isotherms of Au@micro-SiO_2 and Au@meso-SiO_2 are shown in Fig. 3a. The latter exhibited typical type IV behavior, while the former exhibited a small non-characteristic hysteresis loop, which may have resulted from the stacking of particles. Pore size distributions determined by the Barrett-Joyner-Halenda (BJH) method (Fig. 3b) indicated that Au@meso-SiO_2 had an average pore size of 2–3 nm. This likely

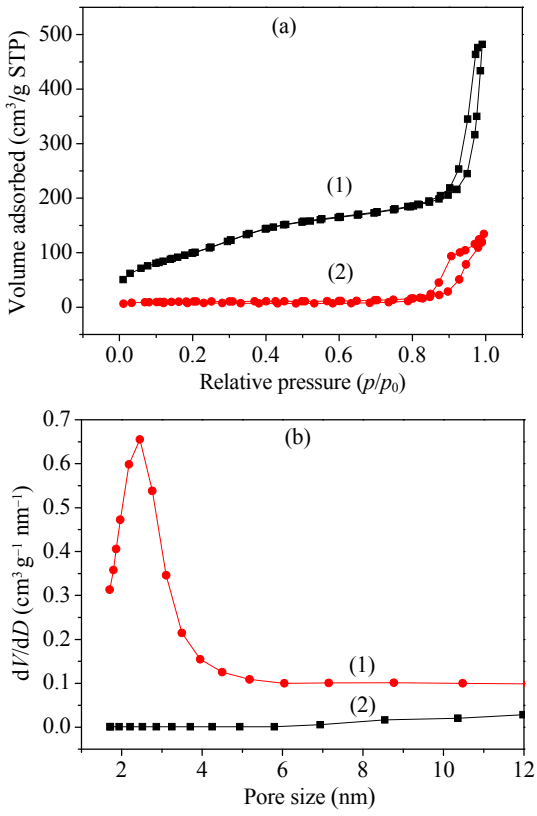

Fig. 3. N_2 adsorption-desorption isotherms (a) and the pore size distributions (b) for Au@meso-SiO_2 (1) and Au@micro-SiO_2 (2).

resulted from the SiO_2 shells and could not have been due to particle stacking. Au@micro-SiO_2 exhibited no pore size of 1–12 nm. The BET surface area of Au@meso-SiO_2 was 368.7 m^2/g, which was much larger than that of Au@micro-SiO_2 (35.3 m^2/g). Because the Au core sizes of the two samples were similar, the different BET surface areas indicated a higher SiO_2 shell porosity in Au@meso-SiO_2.

Figure 4 indicates that Au@meso-SiO_2 had a higher CO oxidation activity than Au@micro-SiO_2. The activity of Au@meso-SiO_2 was comparable to that exhibited by Au@hollow ZrO_2 pre-calcined at 800 °C (Au particle size of 6.3 nm) [21]. SiO_2 and ZrO_2 are both non-reducible. This means that Au@meso-SiO_2 and Au@hollow ZrO_2 are less active for CO oxidation at low temperatures than Au/TiO_2 and Au/Fe_2O_3 because TiO_2 and Fe_2O_3 are reducible. The SiO_2 and ZrO_2 encapsulated Au NPs are durable against sintering at 550–800 °C. The activity of typical

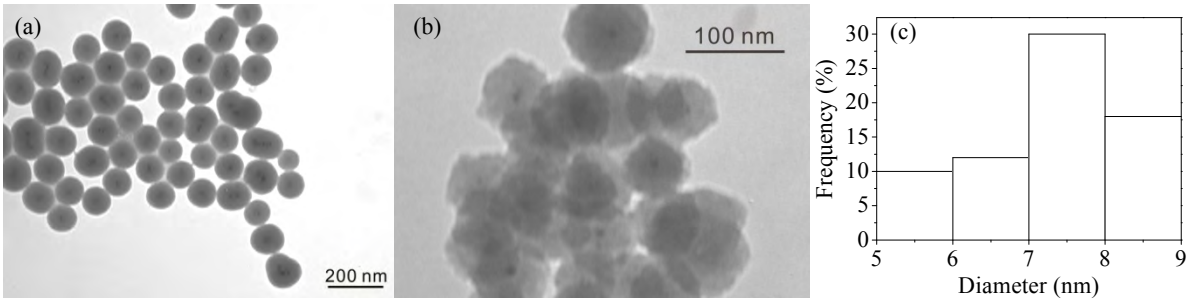

Fig. 2. TEM images of Au@micro-SiO_2 (a) and Au@meso-SiO_2 (b), and Au core size distribution in Au@meso-SiO_2 (c).

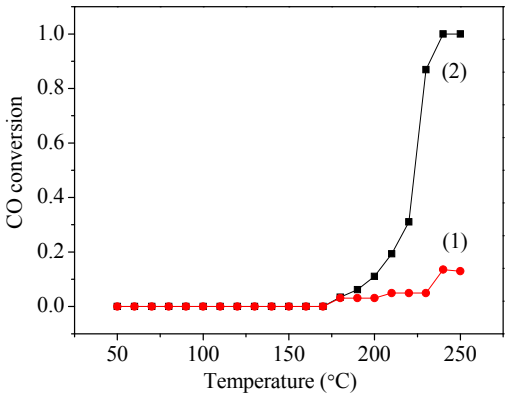

Fig. 4. Catalytic activity for CO oxidation over Au@micro-SiO_2 (1) and Au@meso-SiO_2 (2) calcined at 550 °C.

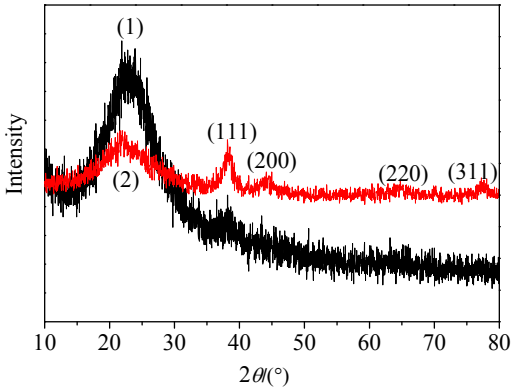

Fig. 5. XRD patterns of Au@micro-SiO_2 (1) and Au@meso-SiO_2 (2).

supported Au NPs depends on the type and structure of the support [38–43]. The mobility of supported Au NPs is rather high, resulting in their tendency to aggregate at low temperatures, and even at RT [44–48]. Thus, reported highly active supported Au NPs have not generally been subjected to calcination, and their activity cannot be maintained for long periods [49–52].

In Au@micro-SiO_2, the limited SiO_2 porosity and strong interaction between Au and SiO_2 hindered CO and O_2 from reaching the Au core surface and undergoing reaction. XRD patterns of Au@micro-SiO_2 and Au@meso-SiO_2 are shown in Fig. 5. The former exhibited weak Au diffractions despite the similar Au particle size of these two samples (Fig. 2). Denser SiO_2 shells in Au@micro-SiO_2 may have weakened the diffraction by Au. The lower density SiO_2 shells in Au@meso-SiO_2 resulted in a weak interaction between Au and SiO_2 and consequently an enhanced diffraction by Au. This resulted in the strong diffraction by Au (2θ = 38.25°, 44.46°, 64.69°, and 77.71°).

Pt@micro-SiO_2 and Pt@meso-SiO_2 core-shell materials were also prepared. TEM images (Fig. 6) show that the average Pt particle size was 8.6 ± 1.5 nm. Multi-core encapsulation in Pt@micro-SiO_2 and aggregation of Pt cores was apparent in some core-shell particles, but the overall structures remained monodisperse. Specific surface areas of Pt@meso-SiO_2 and Pt@micro-SiO_2 were 247.5 and 67.6 m^2/g, respectively. N_2 sorption isotherms (not shown) confirmed that the presence of C_{18}TMS modified the SiO_2 shell texture.

In summary, the "core to shell" strategy was used to fabricate the Ag, Au, and Pt@SiO_2 core-shell nanostructures with core sizes of 5–9 nm, narrow size distributions, and monodisperse structures. The presence of C_{18}TMS resulted in mesoporous SiO_2 shells. This favored mass transport through the shells, and adsorption and reaction on the core surfaces.

3.2. M@SiO_2 (M = Ag and Au) obtained through the "shell then core" approach

3.2.1. Preparation of hollow SiO_2 spheres

The mechanism of hollow SiO_2 sphere formation is related to the presence of the C_{12}-SH and CTAB [23]. C_{12}-SH is hydrophobic and partially dissociates in strongly alkaline solution. C_{12}-S^- electrostatically interacts with CTA^+ to form a supramolecular complex, which is dispersed as a microemulsion in the aqueous phase. TEOS is hydrolyzed in the alkaline medium to form SiO_2 oligomers, which self-assemble with CTA^+ at the C_{12}-S^-/CTA^+ supramolecular interface. The cross-linking oligomerization of TEOS on the interface generates mesoporous SiO_2 spheres. Hydrophobic C_{12}-SH can increase the expansion of CTAB in the microemulsion, which results in SiO_2 spheres of higher porosity. The colloidal SiO_2 sol is then subjected to repeated dispersion in ethanol/water and centrifugation to remove C_{12}-SH and CTAB. Mesoporous SiO_2 spheres are then obtained.

The N_2 adsorption-desorption isotherm and pore size distribution of hollow SiO_2 spheres are shown in Fig. 7. The specific surface area was 533.9 m^2/g, and the isotherm exhibited typical type IV behavior. The average pore size determined by the BJH method was around 3 nm (Fig. 7b).

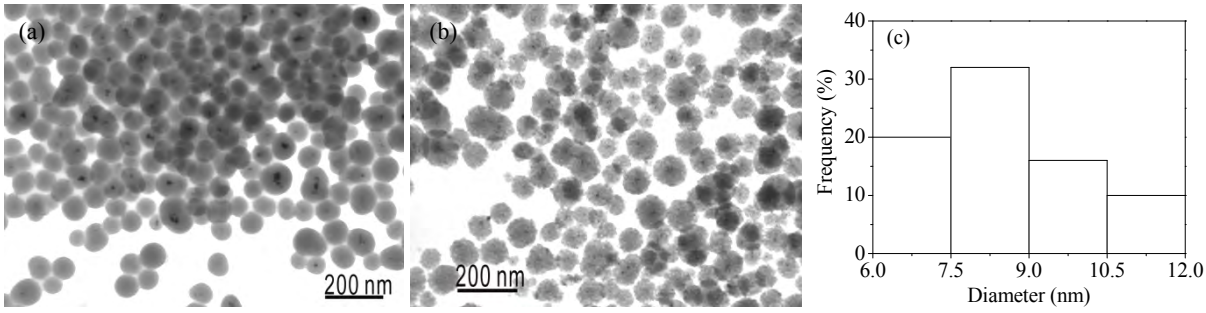

Fig. 6. TEM images of Pt@micro-SiO_2 (a) and Pt@meso-SiO_2 (b), and Pt core size distribution in Pt@meso-SiO_2 (c).

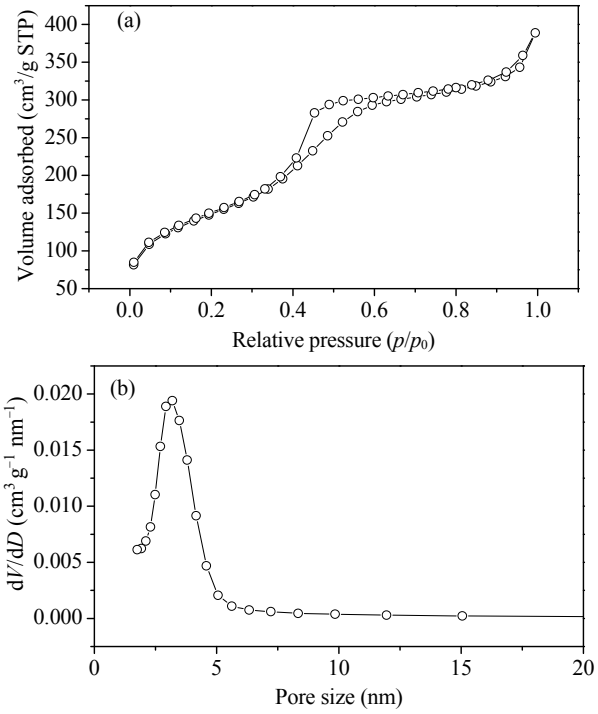

Fig. 7. N_2 adsorption-desorption isotherms (a) and pore size distribution (b) of hollow SiO_2 spheres.

3.2.2. *Fabrication of Au@SiO₂ and Ag@SiO₂*

SiO_2 is non-reducible and cannot reduce metal ions to their corresponding elements. It is necessary to modify SiO_2 shells with functional groups to enable reduction. TSD was employed as a second Si source in this study. TSD hydrolyzes faster than TEOS in alkaline solution. Early in SiO_2 formation, most TSD and some TEOS were co-hydrolyzed and condensed, producing the inner part of SiO_2 spheres. The outer part largely formed during the subsequent hydrolysis and condensation of TEOS. Most TSD was hydrolyzed in the core space, so –NH–CH_2–CH_2–NH_2 functional groups were largely located there. Thus, Au^{3+} and Ag^+ were predominantly reduced inside the SiO_2 spheres as metal cores. TEM images of Ag@SiO_2 and Au@SiO_2 core-shell structures synthesized via the "shell then core" approach are shown in Fig. 8. The average Ag and Au core sizes were 8.0 ± 1.0 nm and 8.5 ± 0.9 nm, respectively. The outer diameter of the hollow SiO_2 spheres was about 80–90 nm. The shells of Ag@SiO_2 were more porous, and the hollow spaces more commodious. This observation was consistent with XRD results (not shown), in which the XRD diffraction of the SiO_2 shell was weak in the pattern of Ag@SiO_2 and strong in that of Au@SiO_2.

3.3. *Catalytic reduction of 4-NP over Au@meso-SiO₂ obtained through the "shell then core" approach*

The blank test indicated that 4-NP could not be reduced in the absence of catalyst, even after 24 h. 4-NP underwent continuous reduction upon the addition of Au@meso-SiO_2 obtained through the "shell then core" approach (Fig. 9). The intensity of the characteristic absorption band of 4-NP at 401 nm decreased with increasing reaction time. The intensity of the

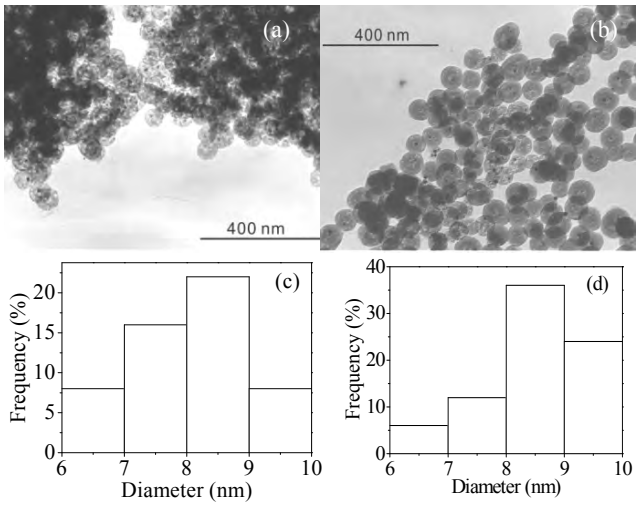

Fig. 8. TEM images of Ag@ SiO_2 (a) and Au@SiO_2 (b) obtained via the "shell then core" approach, and size distributions of the Ag (c) and Au (d) cores.

4-aminophenol absorption at 300 nm correspondingly increased. 4-NP was essentially reduced after reaction for 28 min. The reaction rate constant was obtained from the time dependence of absorbance at 401 nm.

Figure 9b shows that the reaction was first-order with respect to 4-NP. The rate constant was determined from the gradient to be 1.69 × 10^{-3} s^{-1}. After reaction, the catalyst was iso-

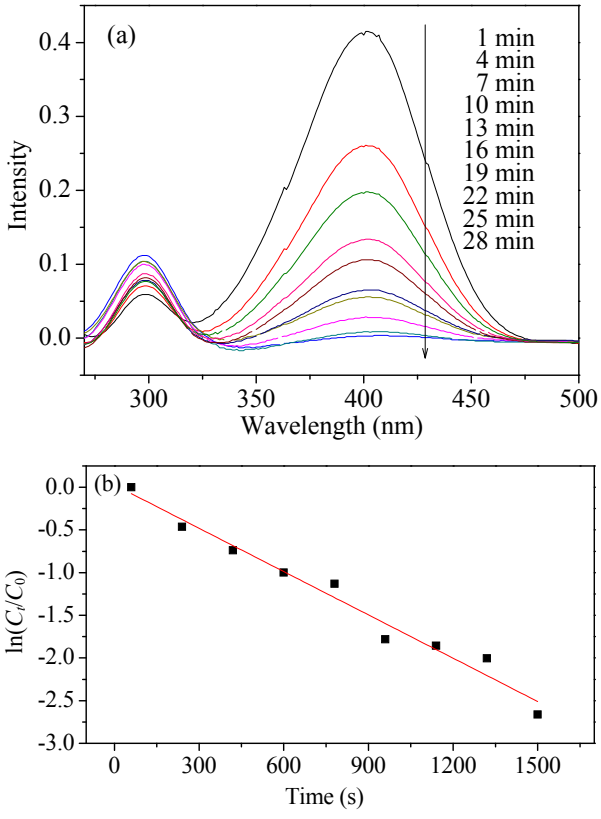

Fig. 9. (a) UV-Vis absorption spectra of the reaction mixture after different times; (b) Time dependence of ln(C_t/C_0) in the presence of Au@SiO_2.

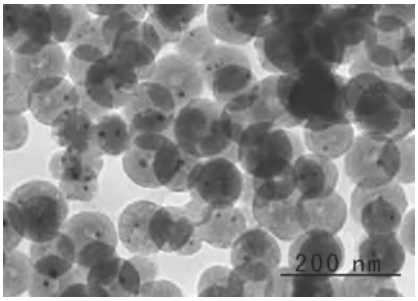

Fig. 10. TEM image of Au@SiO_2 after four cycles.

lated by centrifugation and used for three further 4-NP reduction cycles. No deactivation of catalyst was observed. The used catalyst was finally isolated and analyzed by TEM. The image (Fig. 10) suggested that the core-shell structure was maintained. The Au@meso-SiO_2 core-shell catalyst derived through the "shell then core" approach was highly active and stable. 4-NP could efficiently transport through the mesoporous SiO_2 shell to adsorb and react on the core surface.

4. Conclusions

The "core to shell" and "shell then core" approaches were used to synthesize Ag, Au, Pt@SiO_2 core-shell nanostructures. In the former, Pt, Au, and Ag cores of 6–9 nm diameter were prepared by reduction in ethanol. The surfactant MUA acted as a stabilizing and structure-directing agent, stabilizing the metal NPs in water/ethanol and inducing SiO_2 shell formation on cores through a modified Stöber method. Separating colloidal material from solution by high-speed centrifugation was not required. Employing C_{18}TMS allowed the mesoporous SiO_2 shells to form, which facilitated metal-SiO_2 interaction and reactant diffusion. Catalytic CO oxidation was carried out over Au@meso-SiO_2 obtained through the "core to shell" approach. The SiO_2 shell porosity significantly affected catalytic performance. In the "shell then core" approach, mesoporous SiO_2 hollow spheres were prepared by hydrolysis and condensation of TDS and TEOS. Au and Ag cores of < 10 nm in diameter were formed in-situ and were predominantly deposited inside the SiO_2 spheres. The liquid phase reduction of 4-NP over Au@meso-SiO_2 from the "shell then core" approach indicated minimal diffusion limitation of 4-NP, and high activity and durability of the core-shell catalyst. Employing Si sources with differing functionality allowed the SiO_2 shell and metal core properties to be modified with the two approaches, which is beneficial for application.

References

[1] Reiss P, Protiere M, Li L. *Small*, 2009, 5: 154
[2] Guerrero-Martínez A, Pérez-Juste J, Liz-Marzán L M. *Adv Mater*, 2010, 22: 1182
[3] Burns A, Ow H, Wiesner U. *Chem Soc Rev*, 2006, 35: 1028
[4] Chi F L, Guo Y N, Liu J, Liu Y L, Huo Q S. *J Phys Chem C*, 2010, 114: 2519
[5] Jun Y W, Choi J S, Cheon J. *Chem Commun*, 2007: 1203
[6] Zhou S H, Varughese B, Eichhorn B, Jackson G. McIlwrath K. *Angew Chem In Ed*, 2005, 44: 4539
[7] Chen Y M, Yang F, Dai Y, Wang W Q, Chen S L. *J Phys Chem C*, 2008, 112: 1645
[8] Deng Y H, Qi D W, Deng C H, Zhang X M, Zhao D Y. *J Am Chem Soc*, 2008, 130: 28
[9] Lu J L, Fu B S, Kung M C, Xiao G, Elam J W, Kung H H, Stair P C. *Science*, 2012, 335: 1205
[10] Song C, Du J P, Zhao J H, Feng S A, Du G X, Zhu Z P. *Chem Mater*, 2009, 21: 1524
[11] Yu G B, Sun B, Pei Y, Xie S H, Yan S R, Qiao M H, Fan K N, Zhang X X, Zong B N. *J Am Chem Soc*, 2010, 132: 935
[12] Yang P, Zhang W, Du Y K, Wang X M. *J Mol Catal A*, 2006, 260: 4
[13] Huang W Y, Kuhn J N, Tsung C K, Zhang Y W, Habas S E, Yang P D, Somorjai G A. *Nano Lett*, 2008, 8: 2027
[14] Miyamoto M, Kamei T, Nishiyama N, Egashira Y, Ueyama K. *Adv Mater*, 2005, 17: 1985
[15] Li X G, He J J, Meng M, Yoneyama Y, Tsubaki N. *J Catal*, 2009, 265: 26
[16] Sun B, Yu G B, Lin J, Xu K, Pei Y, Yan S R, Qiao M H, Fan K N, Zhang X X, Zong B N. *Catal Sci Technol*, 2012, 2: 1625
[17] Li L, Li Y, Yao Y, Yao L, Ji W J, Au C. *Prog Chem* (李雷, 李彦兴, 姚瑶, 姚良宏, 季伟捷, 区泽棠. 化学进展), 2013, 25: 71
[18] Joo S H, Park J Y, Tsung C K, Yamada Y, Yang P D, Somorjai G A. *Nat Mater*, 2009, 8: 126
[19] Chen Y, Chen H R, Zeng D P, Tian Y B, Chen F, Feng J W, Shi J L. *ACS Nano*, 2010, 4: 6001
[20] Liu J, Qiao S Z, Hartono S B, Lu G Q. *Angew Chem Int Ed*, 2010, 49: 4981
[21] Huang X Q, Guo C Y, Zuo L Q, Zheng N F, Stuky G D. *Small*, 2009, 5: 361
[22] Chen H M, Deng C H, Zhang X M. *Angew Chem Int Ed*, 2010, 49: 607
[23] Ohmori M, Matijevic E. *J Colloid Interface Sci*, 1992, 150: 594
[24] Ryan J N, Elimelech M, Baeseman J L, Magelky R D. *Environ Sci Technol*, 2000, 34: 2000
[25] Graf C, Vossen D L J, Imhof A, van Blaaderen A. *Langmuir*, 2003, 19: 6693
[26] Gorelikov I, Matsuura N. *Nano Lett*, 2008, 8: 369
[27] Park J C, Lee H J, Jung H S, Kim M, Kim H J, Park K H, Song H. *ChemCatChem*, 2011, 3: 755
[28] Hah H J, Kim J S, Jeon B J, Koo S M, Lee Y E. *Chem Commun*, 2003: 1712
[29] Hah H J, Um J I, Han S H, Koo S M. *Chem Commun*, 2004, 8: 1012
[30] Chen D, Li L L, Tang F Q, Qi S. *Adv Mate*, 2009, 21: 3804
[31] Tan L F, Chen D, Liu H Y, Tang F Q. *Adv Mater*, 2010, 22: 4885
[32] Li L, Yao Y, Sun B, Fei Z Y, Xia H, Zhao J, Ji W J, Au C T. *ChemCatChem*, 2013, DOI: 10.1002/cctc.201300537.
[33] Li L, He S C, Song Y Y, Zhao J, Ji W J, Au C T. *J Catal*, 2012, 288: 54
[34] Li L, Lu P, Yao Y, Ji W J. *Catal Commun*, 2012, 26: 72
[35] Yao L H, Shi T B, Li Y X, Zhao J, Ji W J, Au C T. *Catal Today*, 2011, 164: 112
[36] Li Y X, Yao L H, Song Y Y, Liu S Q, Zhao J, Ji W J, Au C T. *Chem Commun*, 2010, 46: 5298
[37] Chen H M, Hu T, Zhang X M, Huo K F, Chu P K, He J H. *Langmuir*, 2010, 26: 13556
[38] Haruta M, Tsubota S, Kobayashi T, Kageyama H, Genet M J, Delmon B. *J Catal*, 1993, 144: 175
[39] Hartua M. *Gold Bull*, 2004, 37: 27
[40] Tsubota S, Cunningham D A H, Bando Y, Haruta M. *Stud Surf Sci Catal*, 1995, 91: 227
[41] Cunningham D A H, Vogel W, Kageyama H, Tsubota S, Haruta M. *J Catal*, 1998, 177: 1

Graphical Abstract

Chin. J. Catal., 2013, 34: 2098–2109 doi: 10.1016/S1872-2067(12)60716-5

Synthesis and catalytic activity of M@SiO_2 (M = Ag, Au, and Pt) nanostructures via "core to shell" and "shell then core" approaches

Shengchao He, Zhaoyang Fei, Lei Li, Bo Sun, Xinzhen Feng, Weijie Ji*
Nanjing University

"Core to shell" and "shell then core" approaches were used to prepare 6–9 nm diameter M@SiO_2 (M = Ag, Au and Pt) with tunable shell porosity for catalytic reactions.

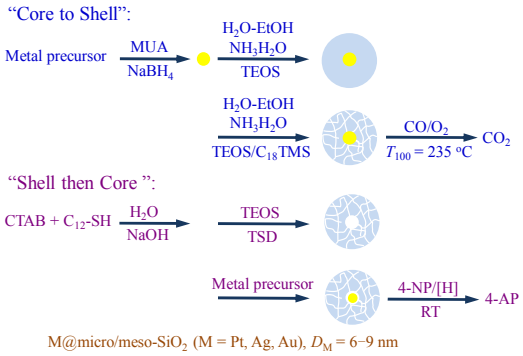

[42] Wolf A, Schüth F. *Appl Catal A*, 2002, 226: 1
[43] Li L, Wang A Q, Qiao B T, Lin J, Huang Y Q, Wang X D, Zhang T. *J Catal*, 2013, 299: 90
[44] Costello C K, Yang J H, Law H Y, Wang Y, Lin J N, Marks L D, Kung M C, Kung H H. *Appl Catal A*, 2003, 243: 15
[45] Akita T, Lu P, Ichikawa S, Tanaka K, Haruta M. *Surf Interface Anal*, 2001, 31: 73
[46] Daté M, Ichihashi Y, Yamashita T, Chiorino A, Boccuzzi F, Haruta M. *Catal Today*, 2002, 72: 89
[47] Schumacher B, Plzak V, Kinne M, Behm R J. *Catal Lett*, 2003, 89: 109
[48] Zanella R, Louis C. *Catal Today*, 2005, 107-108: 768
[49] Vogel W, Cunningham D A H, Tanaka K, Haruta M. *Catal Lett*, 1996, 40: 175
[50] Schubert M M, Plzak V, Garche J, Behm R J. *Catal Lett*, 76: 143
[51] Konova P, Naydenov A, Venkov Cv, Mehandjiev D, Andreeva D, Tabakova T. *J Mol Catal A*, 2004, 213: 235
[52] Moreau F, Bond G C. *Appl Catal A*, 2006, 302: 110

"先核后壳"和"先壳后核"的简便途径制备M@SiO_2 (M = Ag, Au, Pt)纳米核壳结构及其催化活性

何圣超, 费兆阳, 李 雷, 孙 博, 冯新振, 季伟捷*
南京大学化学化工学院介观化学教育部重点实验室, 江苏南京210093

摘要: 采用简便的"先核后壳"和"先壳后核"途径制备了M@SiO_2 (M = Ag, Au, Pt)核壳结构. 采用"先核后壳"途径时,金属内核可以控制在6–9 nm, 粒径分布均匀, SiO_2壳层织构可调. 该途径制备过程简便, 无需高速离心分离, 可有效节约制备成本. 由该途径制得的Au@mSiO_2中纳米Au的热稳定性高, 经550 °C空气焙烧后仍能保持高的CO氧化性能(T_{100} = 235 °C). 由"先壳后核"途径制得的核壳结构内核金属粒子也可以控制在< 10 nm, 粒径分布均匀, 且SiO_2壳层孔隙率可以预调, 即使在液相中也可有效消除对硝基苯酚反应物分子的扩散限制, 并于室温下将其还原为对氨基苯酚. 两种途径所得的核壳结构均呈高单分散态. 使用含有不同有机官能团的硅源可对介孔SiO_2壳层进行进一步改性, 拓展应用领域, 因而具有很好的潜在应用前景.

关键词: 核壳结构; 银; 金; 铂; 纳米粒子; 二氧化硅; 一氧化碳氧化; 对硝基酚还原

收稿日期: 2013-08-30. 接受日期: 2013-09-22. 出版日期: 2013-11-20.
*通讯联系人. 电话: (025)83686270; 传真: (025)83317761; 电子信箱: jiwj@nju.edu.cn
基金来源: 国家自然科学基金(21173118); 江苏省自然科学基金(BK2011439); 高等学校博士学科点专项科研基金(20110091110023); 国家高技术研究发展计划(863计划, 2013AA031703).
本文的英文电子版由Elsevier出版社在ScienceDirect上出版(http://www.sciencedirect.com/science/journal/18722067).

1. 前言

纳米粒子随着粒径的减小, 比表面积急剧增大, 表面能也随之上升, 使纳米粒子容易团聚, 从而失去其内在特性. 同时, 在许多应用领域, 都要求纳米粒子具有复合功能, 因此复合纳米材料的合成成为当前纳米科技发展的研究热点, 其中纳米核壳结构材料是重要的研究领域之一. 核壳结构纳米材料独特的结构使人们能够在纳米尺度上对材料结构和组成进行设计和剪裁, 从而使核壳结构纳米材料具有令人瞩目的特性, 因此在半导体[1]、生物技术[2,3]和药物输送[4,5]等领域具有非凡的潜在应用价值. 近年来, 利用纳米组装技术将纳米粒子组装成核

壳结构催化材料成为催化领域中的研究热点, 发展了诸如金属@金属[6,7]、金属@氧化物[8,9]、金属@碳材料[10,11]、金属@聚合物[12,13]及金属@分子筛[14–16]等不同类型与组成的核壳结构催化剂, 以及它们在诸多催化反应中的应用[17].

SiO_2作为一种传统的包裹材料得到了广泛研究. 一方面, SiO_2具有高的稳定性, 可以有效地保护金属内核粒子的聚集, 而且硅壳层孔隙率可以调控; 另一方面, SiO_2能与氨基、羟基和羧基等有机基团相连接, 使得它在生物方面的应用潜力巨大, 而且SiO_2前驱体容易得到. 这使得SiO_2成为改性纳米材料表面性质并保持金属内核材料特性的一种理想选择. SiO_2包裹的金属纳米颗粒被广泛地应用于胶体与材料科学领域[18–20]. 人们通过溶胶-凝胶法合成了不同形状、尺寸金属核的核壳结构[18,21,22]. 三氧化二铁[23]、二氧化锆和二氧化钛[24]等纳米粒子, 由于在液相合成后表面含有大量羟基, 所以通过水解-缩合可以直接包裹SiO_2层. 然而, 贵金属等纳米粒子则需要通过特定的保护剂、修饰剂、硅偶联剂等来调节金属表面亲水性, 才能有效包裹上SiO_2层. 合成过程比较复杂, 且制备方法扩展应用性较差. Graf等[25]采用聚乙烯吡诺烷酮(PVP)作为修饰剂合成出金属纳米粒子核壳结构, 该方法适用于Au, Ag等金属及Al_2O_3@SiO_2核壳结构的制备. 然而, 对粒径较小(< 8 nm)的金属颗粒则难以制备核壳结构. Matsuura等[26]采用十六烷基三甲基硅烷(CTAB)作为稳定剂和结构导向剂在水相中合成出金属@SiO_2核壳材料, 该制备方法合成出的材料分散性较好, 而且硅壳层具有介孔结构, 有利于扩散传质. 然而该方法合成时间长, 需要高速离心分离, 技术要求与制备成本都比较高. 最近, 有报道采用反相微乳液法合成金属纳米核壳结构[27], 材料分散性好, 硅层厚度可控. 然而反应过程需用大量有机溶剂和表面活性剂, 所以制备成本高且后处理难.

Huang等[21]采用十一硫醇作为稳定剂, 通过有机液相反应合成出6.3nmAu颗粒, 并进一步采用1-巯基十一烷酸(MUA)作为表面修饰剂, 使Au颗粒呈表面亲水性, 再通过改性Stöber方法合成出Au@SiO_2核壳结构, 产物分散性和均匀性高. 本研究的制备策略之一是直接采用MUA, 既作为稳定剂又作为修饰剂, 免去使用十一硫醇, 并在乙醇相中首次合成出金属纳米颗粒, 再在醇-水混合相中通过改性Stöber方法直接在金属粒子表面包裹上一层SiO_2壳层.

核壳结构的制备通常采用上述“先核后壳”的方法. 由于纳米金属核颗粒尺寸小, 表面能高, 所以制备出来的金属核溶胶浓度低, 制备效率低. 近年来开始尝试探索“先壳后核”制备方法, 即先合成出SiO_2壳层, 然后再引入金属纳米核. Hah等[28,29]采用苯基三甲基硅烷作为硅源, 通过调节溶液pH值, 形成空心SiO_2球, 然后再采用超声浸渍方法, 使硝酸铜溶液填充空心SiO_2层内部, 再加入水合肼将Cu^{2+}还原成Cu原子而形成内核金属粒子. 重复浸渍-还原步骤可使内核Cu粒子逐渐长大. 但是, 该方法采用外加还原剂还原硝酸铜, 在形成纳米Cu核的同时, 也有大量的Cu金属离子在壳层外被还原并沉积于SiO_2壳层外表面, 结构均匀性难以保证. 近期, Chen等[30]以及Tan等[31]试图对“先壳后核”途径进行改进, 采用3-(2-氨乙基)-3-氨丙基甲氧基硅烷(TSD)和正硅酸四乙酯(TEOS)两种硅源, 形成SiO_2@TSD+SiO_2@SiO_2夹心层核壳结构, 然后再用HF刻蚀, 利用不同硅层刻蚀速率不同刻蚀掉中间层, 最终形成SiO_2@SiO_2蛋黄型核壳结构, 再通过HF刻蚀, 形成SiO_2空心球. 由于在空腔内壁表面含有大量乙二胺基官能团, 加入适量的$HAuCl_4$, 可以原位还原形成Au纳米粒子, 且Au粒大小可通过$HAuCl_4$浓度进行调变. 然而, 由于空心SiO_2球需通过HF刻蚀得到, 不仅对硅源选择比较苛刻, 而且环境不友好, 具有较大的局限性. 本研究的制备策略之二是免去HF刻蚀, 直接合成出具有空心结构的SiO_2球, 然后通过原位还原得到纳米Au、Ag内核粒子. 因此, 本研究的宗旨是经“先核后壳”和“先壳后核”两种途径, 采用简化步骤制备单分散Pt, Au和Ag@SiO_2纳米核壳结构, 提高合成效率, 同时降低制备成本, 以期发展具有一定普适性的金属@SiO_2核壳材料的简便合成方法. 本文通过两种途径制备了核壳结构M@SiO_2 (M = Ag, Au, Pt), 并选取Au@SiO_2作为代表性体系初步考察了催化性能. 对于由“先核后壳”途径制备的Au@meso-SiO_2, 选择气-固相催化氧化CO探针反应, 了解具核壳结构纳米Au的稳定性; 作为对照, 对于由“先壳后核”途径制备的Au@meso-SiO_2, 选择液-固相催化还原对硝基酚(4-NP)探针反应, 了解介孔SiO_2包裹层对液相中反应物分子扩散限制的影响.

过去几年里, 我们通过制备一系列氧化物纳米粒子前体(包括Fe_2O_3, NiO, Co_3O_4和RuO_2等), 再将其用SiO_2和Al_2O_3等壳层包裹, 然后原位氢还原制备了M@SiO_2和Al_2O_3核壳结构并应用于氨分解及甲烷临氧重整等反应[32–36]. 与我们前期研究不同的是, 本研究涉及的壳层包裹是在金属粒子上直接完成的.

2. 实验部分

2.1. “先核后壳”策略

首先在保护剂和表面修饰剂作用下, 通过液相还原反应合成出金属纳米颗粒, 再通过改性的Stöber法制备SiO_2壳层. 采用1-巯基十一烷酸(MUA)作为保护剂稳定分散在乙醇-水混合溶液中的Au, Ag和Pt纳米粒子, 并诱导SiO_2在其金属纳米颗粒表面形成壳层. 同时采用扩孔剂调控壳层孔隙率, 进而调变核壳结构的扩散性能.

2.1.1. Ag@SiO_2的制备

在30 ml乙醇溶液中加入4 mg $AgNO_3$和1 mg MUA, 于室温下搅拌10 min, 然后滴加5 ml新制备的$NaBH_4$溶液(8.0×10^{-2} mol/L), 快速搅拌10 min, 可观察到溶液颜色立刻从无色变为橘红色, 说明有Ag纳米粒子生成. 再加入2 ml $NH_3\cdot H_2O$和10 ml H_2O, 继续搅拌10 min, 可观察到溶液保持透明, 无沉淀物析出, 再缓慢滴加10.5 ml TEOS溶液(含0.5 ml TEOS和10 ml乙醇), 搅拌6 h, 最终将胶体溶液置于烘箱中, 在80 ºC下蒸发3 h, 得到最终产物.

2.1.2. Pt@SiO_2的制备

在30 ml乙醇溶液中加入1 ml $H_2PtCl_6\cdot6H_2O$溶液(1.93×10^{-2} mol/L)和0.5 mg MUA, 于室温下搅拌10 min, 然后分三次共滴加4.5 ml新制备的$NaBH_4$溶液(8.0×10^{-2} mol/L), 超声30 min, 可观察到溶液颜色从淡黄色逐渐转变为深棕色, 说明有Pt纳米粒子形成. 再滴加2 ml NaOH溶液(0.625 mol/L), 搅拌10 min, 可观察到溶液中有沉淀物生成, 然后通过离心(4000 r/min, 5 min)或者静置30 min, 分离出固体沉淀物, 再加入2 ml $NH_3\cdot H_2O$, 10 ml H_2O和30 ml乙醇, 搅拌30 min, 可观察到沉淀物又分散至透明, 再缓慢滴加10.5 ml TEOS溶液(含0.5 ml TEOS和10 ml乙醇),搅拌6 h, 最终将胶体溶液置于烘箱中, 在80 ºC下蒸发3 h, 得到最终产物.

2.1.3. Au@SiO_2的制备

在30 ml乙醇溶液中加入2 ml $HAuCl_4\cdot4H_2O$溶液(9.7×10^{-3} mol/L)和2.0 mg MUA, 于室温下搅拌10 min, 然后滴加5 ml新制备的$NaBH_4$溶液(8.0×10^{-2} mol/L), 快速搅拌10 min, 可观察到溶液颜色从无色变为酒红色, 说明有Au纳米颗粒形成. 再滴加2 ml NaOH (0.625 mol/L)溶液, 搅拌10 min, 观察到溶液中有沉淀物生成, 然后通过离心分离(4000 r/min, 5 min)或者静置30 min, 分离出固体沉淀物, 再加入2 ml $NH_3\cdot H_2O$, 10 ml H_2O和30 ml EtOH, 搅拌30 min, 可观察到沉淀物又分散至透明, 再缓慢滴加10.5 ml TEOS溶液(含0.5 ml TEOS和10 ml乙醇), 搅拌6 h, 最终将胶体溶液置于烘箱中, 在80 ºC下蒸发3 h, 得到最终产物.

2.1.4. SiO_2壳层改性

合成步骤与Au@微孔-SiO_2和Pt@微孔-SiO_2核壳结构材料相同, 只是最后一步在加入硅源TEOS时同时加入一定量C_{18}TMS, 进行硅层孔隙率改性.

2.2. “先壳后核”策略

通过微乳液法先制备出SiO_2纳米空心球, 并采用不同的硅源对其进行修饰, 合成出具有弱还原性的介孔SiO_2纳米空心球; 然后再通过原位还原方法合成金属Au和Ag等内核纳米粒子.

2.2.1. 空心SiO_2球的制备

参照在水相中制备介孔SiO_2球的方法[37]制备空心SiO_2球. 在100 ml H_2O中分别加入0.2 g CTAB, 40 μl C_{12}-SH和0.7 ml NaOH (2mol/L)溶液, 在80 ºC下搅拌30 min, 使其分散均匀; 再将2 ml TEOS和0.1 ml TSD溶于5 ml乙醇中, 混合均匀后快速搅拌下再逐滴加入到上述溶液中, 观察到有白色溶胶形成; 搅拌3 h后, 再通过离心分离, 并将最终产物在100 ºC下恒温烘干.

2.2.2. Au@SiO_2的制备

取0.2 g空心SiO_2样品均匀分散于50 ml H_2O中, 再加入4 ml $HAuCl_4$溶液(9.712×10^{-3} mol/L), 在室温下超声1 h, 然后再在80 ºC下静置3 h, 可观察到溶液由淡黄色逐渐变成紫红色, 再通过离心分离(4000 r/min, 30 min)并于100 ºC下恒温烘干.

2.2.3. Ag@SiO_2的制备

取0.2 g空心SiO_2样品均匀分散于50 ml H_2O和5 ml乙醇混合液中, 再加入0.1 g $AgNO_3$, 超声溶解, 然后在80 ºC恒温水浴中搅拌12 h, 可观察到溶液逐渐从乳白色变为深黄色, 再离心分离(4000 r/min, 30 min),并于100 ºC下恒温烘干.

2.3. 材料表征

BET比表面积测定在NOVA-1200型材料物理结构测试仪上进行. 样品于300 ºC下脱气3 h, N_2吸附-脱附在–196 ºC进行. X射线衍射(XRD)在Philips X’Pert MPD Pro型X射线衍射仪上进行, Cu K_α射线(λ = 0.1541 nm), 石墨滤波器, X射线管电压为40 kV, 电流为40 mA, 扫描步速0.02º, 扫描范围10º–80º. 透射电镜(TEM)观察在JEM-1010 TEM型透射电镜上进行, 电压80 kV.

2.4. 催化性能评价

对于CO氧化反应, 催化剂用量50 mg (20–40目), 反

应气为CO混合气(1.4%CO + 98.6%空气), 流速25 ml/min, 空速(SV)30000 $cm^3\ h^{-1}\ g_{cat}^{-1}$. 反应前将催化剂样品先于550 ºC焙烧2.5 h, 反应后气体由在线色谱(GC122型色谱仪)检测, Poropak Q检测柱, 热导检测器, 高纯He载气.

对于对硝基酚还原反应, 室温下, 将10.0 mg Au@SiO_2分散在5 ml H_2O中, 再加入1 ml $NaBH_4$ (0.3 mol/L)溶液, 搅拌10 min至均匀, 再加入0.2 ml 4-NP (7.62×10^{-2} mol/L), 快速搅拌至溶液从淡黄色变为无色. 反应过程中每隔3 min取0.1 ml反应液, 加水稀释至4 ml, 并在UV-Vis分光光度计上测定其吸收峰强度变化, 并据此计算催化反应活性.

3. 结果与讨论

3.1 "先核后壳"策略制备M@SiO_2 (M = Ag, Au, Pt)

由于贵金属胶体粒子表面含亲水官能团较少, 亲水性较弱, 所以需要加入表面活性剂或硅烷偶联剂对其表面进行改性. 作为重要的改进尝试, 我们于金属纳米粒子形成之前加入MUA, 既作为金属纳米粒子的稳定剂, 又作为结构导向剂对其金属表面进行改性, 增加金属表面亲水性, 从而使SiO_2壳层能容易地覆盖在金属表面上. 据我们所知, 这是首次在醇溶液中直接利用MUA作为保护剂和稳定剂合成出小于10 nm的金属纳米粒子. 图1为Ag@SiO_2核壳结构的TEM照片及Ag核粒径分布图, 其中Ag核粒径平均尺寸为5.7 ± 0.5 nm, SiO_2层厚度在40–50 nm, 基本呈单核包裹且分散性很好.

为了验证该合成过程具有一定的普适性, 按照同样的合成步骤, 成功制备了Au@SiO_2核壳纳米结构, 如图2所示. Au核平均尺寸为7.3 ± 1.0 nm. 部分核壳结构呈现多核包裹, 即一个核壳结构内含有2–3个Au粒, 但Au粒并未团聚成一个大粒子, 且仍被SiO_2有效分隔. 在此基础上, 通过加入扩孔剂C_{18}TMS([C_{18}TMS]:[TEOS] = 1:8)进一步调变SiO_2壳层孔隙率, 制备出具有介孔织构的SiO_2壳层(明显疏松的壳层, 见图2b电镜照片). 通过测量Au@micro-SiO_2和Au@meso-SiO_2的吸附等温线(图3a), 前者呈典型的IV型, 后者虽也有小的包络线, 但并不特征, 很可能是核壳粒子形成的堆积孔. 由BJH法确定的二者的孔径分布(图3b)进一步证明后者最可几孔径分布在2–3 nm, 不可能是核壳粒子形成的堆积孔, 因而证明了其SiO_2壳层的介孔结构; 而前者在1–12 nm范围无明显孔径分布. 此外, Au@meso-SiO_2的比表面积达368.7 m^2/g, 远高于Au@micro-SiO_2的比表面积(35.3 m^2/g), 由于二者内核Au粒子尺寸相若, 其比表面积的显著差异也清楚地反映出前者SiO_2壳层的孔隙率明显高于后者.

由图4可以看出, Au@meso-SiO_2的催化活性显著高于Au@micro-SiO_2. 前者的催化活性和Stucky研究组[21]报道的6.3 nm Au@空心ZrO_2核壳材料(可耐受800 °C焙烧处理)的相类似. 由于SiO_2和ZrO_2是不可还原的氧化物, 因此与由可还原载体构成的Au/TiO_2和Au/Fe_2O_3体系相比, 其低温氧化活性不占优势. 然而, SiO_2和ZrO_2壳层包裹的纳米Au催化剂的显著特点是耐高温(550–800 °C)、抗烧结, 而常规的负载纳米Au体系, 一方面其活性强烈依赖于载体种类与结构[38–43], 另一方面由于负载Au粒子的移动性高, 在较低温度甚至室温下都能发生Au粒子的聚集[44–48], 故活性高的负载小粒径纳米Au体系一般不经历焙烧处理, 活性也难以长时间保持[49–52]. Au@micro-SiO_2的SiO_2壳层孔隙率低, 而且SiO_2壳层与Au表面的作用过强, 致使CO/O_2难以到达Au粒表面并发生反应. 比较Au@micro-SiO_2和Au@meso-SiO_2的XRD谱(图5)可以看出, 前者Au核的XRD峰很弱, 而电镜照片显示二者Au核的尺寸非常接近, 这说明Au核衍射峰强弱的不同并非是由于Au粒尺寸的差异. 可能前者SiO_2壳层比较致密, 使X射线与Au核相互作用减弱. 而Au@meso-SiO_2的SiO_2壳层疏松, Au-SiO_2相互作用弱, X射线易与Au核发生相互作用, 从而产生明显的衍射峰(2θ = 38.25º, 44.46º, 64.69º, 77.71º).

以相同的合成策略, 我们也制备了Pt@micro-SiO_2和Pt@meso-SiO_2核壳结构材料. TEM照片(图6)显示, Pt核平均尺寸为8.6 ± 1.5 nm. Pt@micro-SiO_2核壳结构中出现一些多核包裹, 个别Pt核粒子的团聚性要比Au核粒子高, 但SiO_2壳层仍然是单分散的. 比表面积测定(Pt@meso-SiO_2 = 247.5 m^2/g, Pt@micro-SiO_2 = 67.6 m^2/g)以及N_2吸脱附等温线测量(图未示出)证实了使用C_{18}TMS调变SiO_2壳层的有效性. 总体来看, 本研究改进的"先核后壳"合成策略能够成功制备Ag, Au及Pt@SiO_2核壳结构, 内核粒子尺寸 < 10 nm, 粒子尺寸相近, SiO_2包裹层均匀, 通过使用C_{18}TMS扩孔剂, 可以有效调变SiO_2壳层孔隙率以及Au-SiO_2相互作用, 从而有利于吸附和表面反应的进行.

3.2. "先壳后核"策略制备M@SiO_2 (M = Ag, Au)

3.2.1. 空心SiO_2球制备

空心SiO_2球形成机理与C_{12}-SH和CTAB密切相关[23]. C_{12}-SH是憎水性分子, 在强碱性溶液中, 部分C_{12}-SH会脱去H质子形成C_{12}-S^-, 并且与CTA^+离子通过静电作用

形成超分子聚集体, 成为微乳液分散在水相中. TEOS在碱溶液中水解形成SiO_2寡聚物, 并与C_{12}-S^-/CTA^+超分子聚合物中的CTA^+发生自组装; 最终在不同的C_{12}-S^-/CTA^+超分子界面上TEOS同时交联聚合, 形成介孔层状SiO_2球. 在该反应过程中, 憎水性分子C_{12}-SH作为膨胀剂与CTAB相互作用形成微乳液, 并有效提高CTAB表面活性剂的膨胀效应, 能够扩张介孔SiO_2球孔径大小. 将介孔SiO_2溶胶多次在乙醇-水溶液中分散溶解, 再离心分离, 除去C_{12}-SH和CTAB表面活性剂, 最终得到介孔SiO_2空心球.

对所得空心SiO_2球进一步测量其吸脱附等温线和孔径分布, 如图7所示. 空心SiO_2球的比表面为533.9 m^2/g, 吸附-脱附等温线属典型的IV型, 说明具有介孔结构, 由BJH法测得SiO_2壳的孔径分布在3 nm左右(图7b).

3.2.2. Au@SiO_2和Ag@SiO_2合成

SiO_2不具有还原性, 无法将金属盐类还原成单质, 因此需要对SiO_2纳米壳层做进一步修饰改性. 本研究使用一定量TSD作为硅源, 由于在碱性水溶液中TSD的水解速率大于TEOS水解速率, 所以在SiO_2球形成初期, 大部分的TSD与少量TEOS共同水解缩合形成内层, 随后外层主要是由TEOS水解缩合形成, 最终形成介孔SiO_2空心球, 所以绝大部分–NH–CH_2–CH_2–NH_2基团存在于内核位置. 因此, 纳米金属粒子大部分在SiO_2球内腔得以还原从而形成M@SiO_2核壳结构. 图8为“先壳后核”途经制得的Ag@SiO_2和Au@SiO_2纳米结构的电镜照片. 可以看到, Ag核粒子平均尺寸是8.0 ± 1.0 nm, Au核粒子平均尺寸为8.5 ± 0.9 nm. SiO_2空心球外径为80–90 nm, 中心部分大多呈中空状. 前者SiO_2壳层更为疏松, 空腔也更大, 这也为样品的XRD谱所支持(图未示出): 前者SiO_2组分的信号极弱, 而后者的较强.

3.3. Au@SiO_2上4-NP催化还原活性

在没有催化剂时, 24 h内未观察到4-NP被$NaBH_4$还原. 图9显示加入Au@meso-SiO_2后, 在401 nm处的4-NP特征吸收峰不断降低, 与此同时对氨基酚在300 nm处的特征吸收峰不断升高; 对应着4-NP不断被还原成对氨基酚, 28 min后, 4-NP基本被还原. 通过定量计算401 nm处吸收峰强度随时间的变化, 可以得到其反应速率常数, 结果如图9b所示.

由图9b可知该催化反应对4-NP属一级反应, 通过计算直线斜率得到其速率常数为1.69×10^{-3} s^{-1}. 反应结束后, 催化剂Au@SiO_2通过离心分离并重复使用3次, 催化剂仍然保持相同活性. 反应后催化剂的电镜照片(图10)显示Au@SiO_2的核壳结构得以完整保持. 通过液相催化还原4-NP模型反应可以看出, Au@SiO_2核壳结构材料具有优良的催化性能, 且稳定性良好; 反应物分子能有效地扩散通过SiO_2壳层, 并在Au核粒子的表面发生催化转化.

4. 结论

发展了改进的“先核后壳”和“先壳后核”途径制备M@SiO_2 (M = Ag, Au, Pt)核壳结构. 前一途径中金属内核可以控制在6–9 nm, 粒径分布均匀, SiO_2壳层织构可调. 该途径制备过程简便, 无需高速离心分离, 可有效节约制备成本. 后一途径制得的核壳结构内核金属粒子也可以控制在< 10 nm, 粒径分布均匀, 且SiO_2壳层孔隙率可以预调, 即使在液相中也可有效消除反应物分子的扩散限制. 两种途径所得的核壳结构均呈高单分散态. 通过使用含有不同有机官能团的硅源, 可对介孔SiO_2壳层进行进一步改性, 拓展应用领域, 因而具有很好的潜在应用前景.